Mechanism of Formation and Construction of Self-Assembled Myoglobin/Hyaluronic Acid Multilayer Films: An Electrochemical QCM, Impedance, and AFM Study

E. M. Pinto, M. M. Barsan, and C. M. A. Brett*

Departamento de Química, Faculdade de Ciências e Tecnologia, Universidade de Coimbra, 3004-535 Coimbra, Portugal

Received: July 29, 2010; Revised Manuscript Received: September 20, 2010

Self-assembled multilayer films of hyaluronic acid (HA) and the protein myoglobin (Mb) were built up layer by layer on Au covered quartz crystal microbalance (AuQCM) electrode substrates. Film formation and growth were monitored by an electrochemical quartz crystal microbalance (EQCM), and the step-by-step construction was investigated through quantification of the mass variation corresponding to adsorption of each monolayer together with cyclic voltammetry. A decrease of friction at the liquid/electrode interface was observed, indicating that the electrode surface becomes less rough after deposition of several monolayers. The properties of the $\{HA/Mb\}_n$ films were evaluated by electrochemical impedance spectroscopy (EIS). Modeling of the impedance spectra shows smoothing of the modified electrode surface with reorganization of the film structure after few monolayers, and the contribution of each layer to the electron transfer process was analyzed. The smoothing of the surfaces and the structural differences between successive bilayers was confirmed by morphological observations by using atomic force microscopy.

1. Introduction

Recently, many researchers have been devoting special attention to the development of new techniques and methods to construct biocompatible ultrathin films. Among them, layer-by-layer (LBL) assembly has attracted increasing interest.[1,2] This method of film construction involves the alternate adsorption of oppositely charged species from solution onto solid surfaces leading to self-construction. One significant advantage over other methods is the precise control of the layer formation as well as its thickness. It allows for the formation of ultrathin molecular films and can be applied to a large variety of multilayer films.[3] However, the construction of LBL assemblies containing a biomolecule such as a protein requires a good understanding of the mechanism of interaction between the protein and the polyions.[2,3] The effective immobilization of enzymes on solid substrates, without changing the original conformations and bioactivities of the enzymes, is possible and can also be extended to the build-up of protein films with oppositely charged nanoparticles.[4]

LBL self-assembly can play an important role in electrochemistry, such as in studies of redox proteins incorporated in multilayer films.[5,6] In this way, the mechanism of direct electron transfer between proteins and electrodes can be studied, elucidating the mechanism of electron transfer in real biological systems.[7]

Some authors report the use of hyaluronic acid (HA) as a receptor of proteins because of its specific interactions with matrix proteins or cell surfaces.[8] HA has been extensively used in LBL assemblies, mostly together with poly(allylamine) (PAA)[9] and chitosan,[10] and the loading behavior of these films toward myoglobin (Mb) was also studied.[11] The assembly of HA with Mb in $\{HA/Mb\}_n$ films is of interest because of the possibility of studying the interaction between proteins and between proteins and other compounds.[12] However, the development of a viable immobilization method for proteins at the electrodes is difficult, and the mechanism involved in film build-up is still not well clarified.

Some authors report that LBL film growth is linear with the number of bilayers (n), that is, a uniform increase of film thickness, whereas some recent reports show an exponential growth of the film thickness.[13−20] The exponential growth in these cases is explained by taking into account the increase of surface roughness with each layer deposition, leading to an increase in electrode effective area, so that a higher amount of polyion can be adsorbed.[14,15] Nevertheless, other authors consider that the free polyions, which remain in the adsorbed film, may diffuse out from the film in the next adsorption step and combine with oppositely charged species on the film surface, leading to an increase of the amount of adsorbed film.[21] Thus, the understanding of the type of film formation process is a challenge.

A previous paper described the cyclic voltammetric behavior of the $\{HA/Mb\}_n$ films during the film formation and also the stability of the films in time. The electrochemical characteristics of the $\{HA/Mb\}_n$ modified electrode were compared with the response of the electrode in solution containing the Mb or of an electrode modified with a thin layer of Mb, in order to identify the electroactive species and elucidate the electron-transfer mechanism.[22] There were indications of the release of electroactive heme contained by the protein in such LBL structures.

The work described in this article focuses on the mechanism of LBL deposition on gold-covered quartz crystal (AuQCM) substrates. Mb was assembled with the anionic form of HA on an AuQCM substrate, and the factors that may influence the assembly of Mb with HA were investigated systematically. The deposition of Mb in the LBL structures with HA is based on the electrostatic interactions between the positively charged amino-acid residues located at the surface of the Mb at pH 5.0 (the isoelectric point (pI) of Mb is 6.8) and the polyanion derived from HA. HA is a polymer of disaccharides, themselves

* Corresponding author. Tel.: +351-239-835295. Fax: +351-239-827703. E-mail: brett@ci.uc.pt.

10.1021/jp107107b
Published on Web 10/21/2010

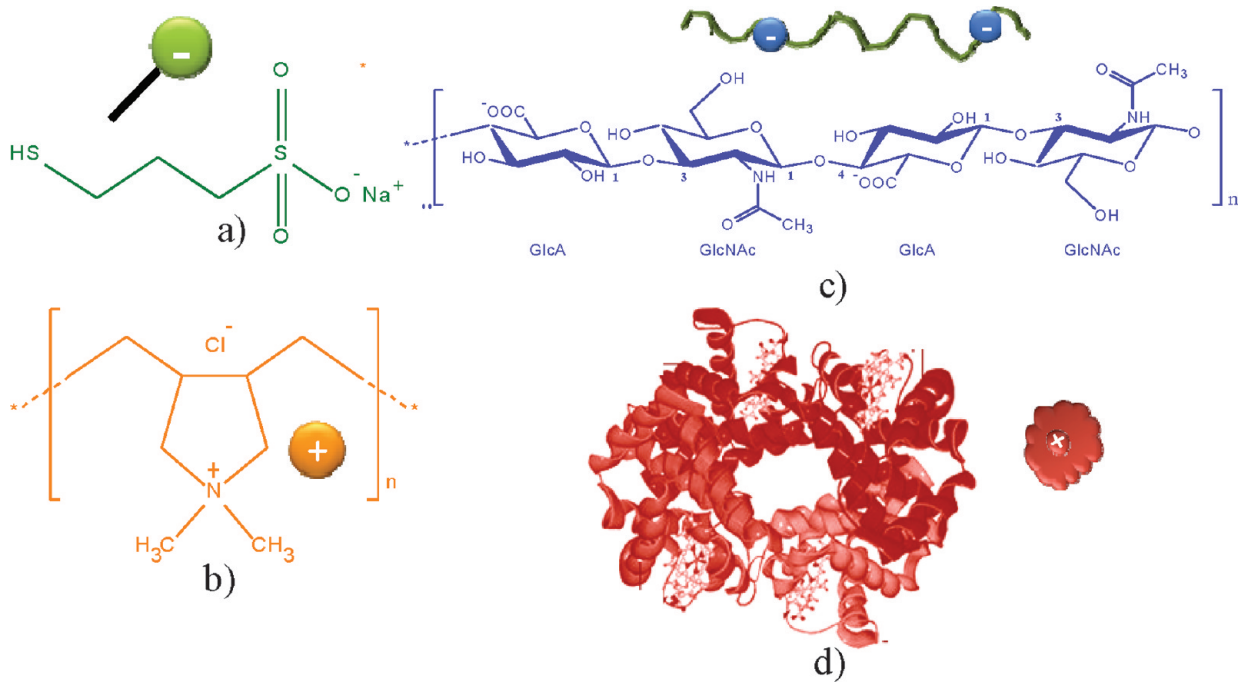

Figure 1. Chemical structures and representations of (a) MPS, (b) PDDA, (c) HA, and (d) Mb.

composed of D-glucuronic acid and D-*N*-acetylglucosamine, linked via alternating β-1,4 and β-1,3 glycosidic bonds. At pH 5.0 ($pK_a = 2.9$), the carboxyl groups of the glucuronic acids are deprotonated so that the polymer will be negatively charged.[22]

The simultaneous gravimetric and voltammetric response of the modified electrodes was used to evaluate the stability of the films, both physical and electrochemical. The electrochemical properties of the HA/Mb modified AuQCM electrodes were evaluated after each bilayer deposition by electrochemical impedance spectroscopy (EIS), and the contribution of each layer to the electron-transfer process was determined by EIS. Both QCM and EIS results suggest a mechanism which initiates with the formation of island-like structures, a nonuniform deposition of the first three bilayers, and then a uniform and homogeneous LBL assembly. Surface characterization by AFM at electrodes modified with 2, 4, and 6 {HA/Mb} bilayers supports the proposed mechanism.

2. Experimental Section

2.1. Chemicals. Sodium 3-mercapto-1-propanesulfonate (MPS, technical grade 90%) and poly(diallyldimethylammonium chloride) (PDDA), very low molecular weight, 35% wt. in water, from Aldrich and HA sodium salt, from *Streptococcus equi. Sp.* was from Fluka and Mb, from horse heart (minimum purity 90%, iron content minimum 0.2%) was from Sigma. All these substances were used as received. The structure of these molecules and their representation are shown in Figure 1. All other chemicals were pro-analysis grade.

The buffer solution used was 0.05 M acetate buffer +0.1 M KBr pH 5.0, prepared by mixing 0.05 M sodium acetate with 0.05 M acetic acid (both from Riedel-deHaën, Germany) and KBr (Merck, Germany).

Potassium bromide electrolyte was chosen to replace the commonly used KCl electrolyte because of the limited potential window at Au electrodes: at potentials above +0.8 V versus SCE, there is the possibility of forming a gold chloride complex ($AuCl_4^-$)[23] which can be dissolved after several cycles, removing the gold film from the electrode surface. The formation of the $AuBr_4^-$ complex is only possible at much higher positive potentials.

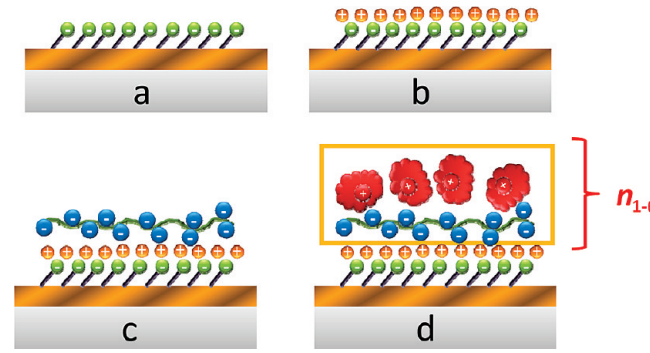

Figure 2. Schematic representation of LBL film construction on AuQCM substrates: (a) AuQCM−MPS(−), (b) AuQCM−MPS(−)/PDDA(+), (c) AuQCM−MPS(−)/PDDA(+) HA(−), and (d) AuQCM−MPS(−)/PDDA(+){HA/Mb}$_1$.

Millipore Milli-Q nanopure water (resistivity ≥18 MΩ cm) and analytical reagents were used for the preparation of all solutions. Experiments were performed at room temperature (25 ± 1 °C).

2.2. Film Assembly. Gold-coated quartz crystals for microbalances (AuQCM) were used as electrodes for both electrochemical and gravimetric studies. Electrodes were prepared from AT-cut piezoelectric quartz crystals (KVG-Germany), 6 MHz with a geometric area of 0.28 cm^2.

Au electrodes were first cleaned with piranha solution (3:1 H_2SO_4 95−97%:7 M H_2O_2), then washed with Milli-Q water, and dried in a N_2 stream during 2 min.

The sequential steps of LBL assembly are shown in Figure 2, (see structures of compounds in Figure 1).

The cleaned electrodes were then immersed for 24 h in 4 mM MPS solution (MPS dissolved in 1:1 ethanol:0.01 M H_2SO_4) to negatively charge the Au surface by the chemical adsorption of an MPS monolayer as shown in Figure 2a. Subsequently, the AuQCM−MPS(−) modified electrodes were

immersed in 3 mg mL^{-1} PDDA in 0.05 M acetate buffer +0.1 M KBr pH 5.0 solution during 20 min and carefully washed and dried in a N_2 stream. In this way, the final precursor-modified electrode was positively charged: AuQCM−MPS(−)/PDDA(+), see Figure 2b. After precursor adsorption, we proceeded with $\{HA/Mb\}_n$ LBL film formation (where n is the number of bilayers) by alternately immersing the electrodes during 20 min in 1 mg mL^{-1} HA (anionic form, Figure 2c) and 1 mg mL^{-1} Mb (Figure 2d), both prepared in 0.05 M acetate buffer +0.1 M KBr pH 5.0 solution. After each deposition step, the electrodes were rinsed with water and dried in a N_2 stream for about 2 min. This cyclic process was followed until the desired number of bilayers (n) was reached.

2.3. Instrumentation. Electrochemical characterization was carried out in a conventional electrochemical cell containing three electrodes, an AuQCM modified electrode as working electrode, a platinum foil as counter electrode, and a saturated calomel electrode (SCE) as reference. Voltammetric measurements were performed by using a computer-controlled μ-Autolab Type II potentiostat-galvanostat running with GPES (general purpose electrochemical system) for Windows version 4.9 software (Metrohm-Autolab, Utrecht, Netherlands).

EIS experiments were carried out by using a PC-controlled Solartron 1250 Frequency Response Analyzer, coupled to a Solartron 1286 Electrochemical Interface using ZPlot 2.4 software (Solartron Analytical, UK), with an rms perturbation of 10 mV applied over the frequency range 65.5 kHz−0.01 Hz, with 10 frequency values per frequency decade. The spectra were recorded at the open circuit potential (OCP), measured just before each EIS experiment.

Gravimetric studies were performed by using a homemade electrochemical quartz crystal microbalance (EQCM), without recording dissipation, connected to a μ-Autolab (Metrohm-Autolab, Netherlands), controlled by GPES Autolab software. The mass/frequency correlation factor obtained for the system, according to the Sauerbrey equation,[24] is 3.45 ng/Hz where $\Delta f = -2.91 \times 10^8 \Delta m$.

The pH measurements were carried out with a CRISON 2001 micro pH-meter (Crison, Spain) at room temperature.

AFM was performed with a Multimode TM Atomic Force Microscope controlled by a Digital Instruments Nanoscope E controller (Veeco Instruments, U.S.A.). Silicon nitride Nano-Probe TM V-shaped cantilevers, 100 mm length, 0.58 N m^{-1} spring constant, were used. All images were recorded in contact-mode AFM in air at room temperature.

3. Results and Discussion

3.1. Film Assembly Monitored by QCM. The QCM is an excellent means of monitoring the dynamics of the adsorption process. Associated with other techniques, the QCM allows the measurement, in situ and in real time, of changes in film properties of the LBL $\{HA/Mb\}_n$ assembly. The mass variation in time can be monitored on the basis of the relationship between the induced frequency variation and the deposited mass on the QCM crystal. In the specific case of rigid films adsorbed at the QCM crystal surface, this relationship is described by the Sauerbrey equation:[24]

$$\Delta f = -\frac{2f_0^2}{A\sqrt{\mu_q \rho_q}}\Delta m \qquad (1)$$

where f_0 is the resonant frequency (Hz), Δf is the frequency change (Hz), Δm is the mass change (g), A is the piezoelectrically active crystal area, ρ_q is the density of quartz (2.648 g cm^{-3}), and μ_q is the shear modulus of quartz for AT-cut crystals (2.947×10^{11} g cm^{-1} s^{-2}) which leads to $\Delta f = -2.91 \times 10^8 \Delta m$.

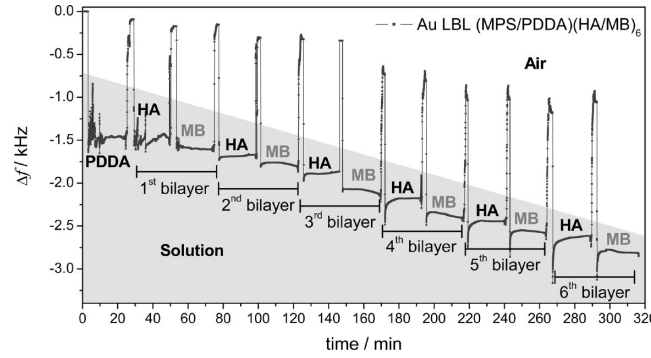

Figure 3. QCM frequency shift during the deposition of PDDA(+) and the alternated deposition of HA(−) and Mb(+) monolayers on AuQCM−MPS(−) modified electrode.

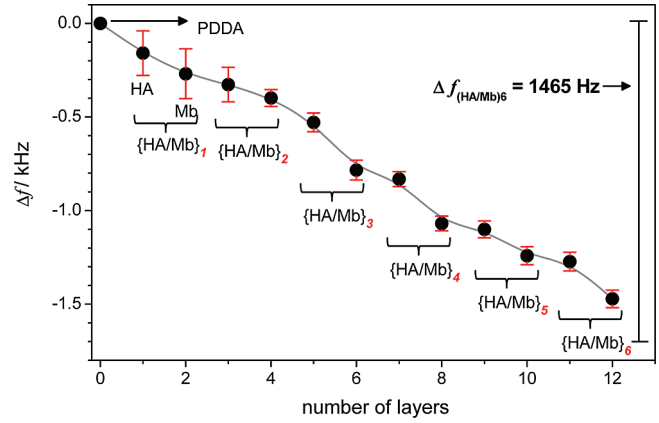

Figure 4. Frequency-shift values calculated after each monolayer deposition on AuQCM−MPS(−) modified electrode with respect to the frequency recorded for the AuQCM−MPS(−)/PDDA(+) modified electrode.

The plot in Figure 3 shows each step of the film formation, after 24 h immersion in MPS solution, as described in the Experimental Section. The AuQCM−MPS(−) modified electrode was cleaned after immersion in order to remove any unadsorbed species and then dried in a N_2 stream. After stabilization, the frequency was recorded, and the value obtained for the AuQCM−MPS(−) modified crystal, oscillating in air, was $f_0 = 6008203$ Hz. The f shift due to AuQCM−MPS(−) immersion in the second precursor (PDDA) solution was 1.47 kHz. In order to simplify the interpretation of the gravimetric plot, the frequency obtained after stabilization of the system AuQCM−MPS(−)/(PDDA)(+) was taken as the reference value to make it easier to follow the change in frequency corresponding to each monolayer deposition. After each adsorption step, the crystal was rinsed with water and dried in a N_2 stream, which caused the frequency peaks in the gravimetric plot.

Figure 3 shows that the first three layers (PDDA(+), HA(−), and Mb(+), to give PDDA(+)$\{HA/Mb\}_1$) deposited nonuniformly, because the deposition process of the first three layers is highly influenced by the formation of microstructures (islands) which are nonhomogeneously distributed on the crystal surface.[17]

Figure 4 shows the frequency-shift values calculated after each monolayer deposition on AuQCM−MPS(−) modified electrode with respect to the frequency recorded at the

TABLE 1: Values of Shift in Frequency and Mass Deposition with Each Monolayer Deposited during the AuQCM−MPS(−)/PDDA(+)/{HA/Mb}$_6$ Construction[a]

number of bilayer	Δ(HA/Mb) Δ*f*/Hz	{HA/Mb}$_n$ Δ*f*/Hz	Δ(HA/Mb) Δ*m*/μg cm^{-2}	{HA/Mb}$_n$ Δ*m*/μg cm^{-2}
1	159/110	269	1.96/1.35	3.31
2	58/72	130	0.71/0.89	1.60
3	130/155	385	1.60/3.15	4.75
4	48/237	285	0.60/2.91	3.51
5	31/141	172	0.38/1.74	2.12
6	32/199	231	0.40/2.45	2.85
total		1470		18.21

[a] The conversion factor for KVG 6 MHz Au−QCM is 3.45 ng/Hz.

AuQCM−MPS(−)/PDDA(+) modified electrode. The corresponding change in values of both frequency and calculated mass are presented in Table 1; such variations in frequency between successive bilayers are always seen, particularly for the first layers. The overall shift in frequency up to the sixth bilayer is 1.47 kHz, which corresponds to a deposited film of 18.2 μg cm^{-2} with an average of 3.04 μg cm^{-2} per {HA/Mb} bilayer. As observed, the deposition of the first three monolayers is not linear; the film begins to be deposited more linearly after this because the electrode surface becomes more uniform. Even so, the film deposition mechanism is less linear than some reports in the literature.

The microbalance used is unable to register the dissipation coefficient. Nevertheless, some experiments were carried out with an oscilloscope connected to the QCM. By analyzing the frequency signal measured with the oscilloscope, positive changes in the signal amplitude were observed. This increase in amplitude is directly associated with *R*', a parameter defined as the electric measure of mechanical dissipation due to loss or gain of energy in each oscillation,[25] indicating a change of viscoelasticity or roughness of the film.

The experiments show that dissipation tended to disappear after the formation of two bilayers and then remained almost constant. For this reason, it was inferred that the dissipations were related to changes in the structure of the layers which can be correlated with the roughness variation seen by AFM imaging (see Section 3.4). Thus, it is assumed that the viscoelastic effects are due to friction at the electrode−liquid interface and not to changes in liquid viscosity.

3.2. Simultaneous Gravimetric and Voltammetric Response of the Modified Electrodes. Cyclic voltammograms were recorded simultaneously with the gravimetric response as shown in Figure 5 in order to correlate the current and frequency changes in the oxidation/reduction processes. It can be seen that the system is electrochemically very stable, the same current amplitude of 165 μA cm^{-2} being recorded for each cycle. After 180 s, the time corresponding to the beginning of the third cycle, the change in frequency shift between cycles is close to zero. This shift is due to a rearrangement of the layers as a result of the oxidation and reduction of the species and to desorption of weakly adsorbed species at the electrode surface after several cycles. The change in frequency shift tends to decrease after three cycles, after desorption of weakly adsorbed species, reaching a constant shift after this. The surface becomes smoother, a decrease of the friction in the interface electrode/electrolyte being observed, explaining the positive shift in the frequency value.

The frequency amplitude for each cycle also maintained the same value of 5.9 ± 0.3 Hz, meaning that no loss or gain in mass occurs, confirming the stability of the LBL modified

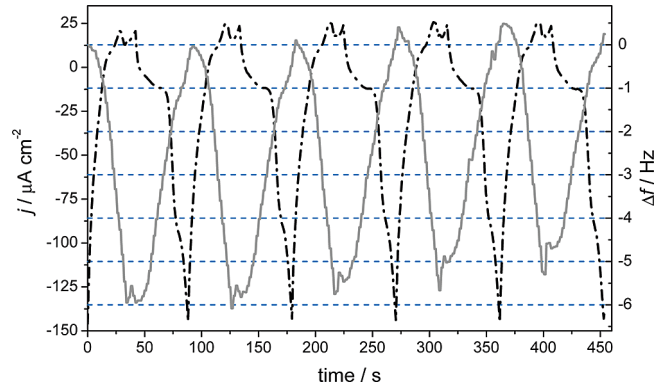

Figure 5. Gravimetric(-) and voltammetric(--) response of the AuQCM−MPS(−)/PDDA(+)/{HA/Mb}$_6$ electrode, recorded in 0.05 M acetate +0.1 M KBr buffer solution pH 5.0; scan rate 5 mV s^{-1}.

electrode. With each cycle, both minimum and maximum frequency values increase slightly, attributed to the reorganization of the deposited species at the electrode after each redox process, resulting in a decrease in the friction at the electrode/electrolyte interface.

3.3. EIS. EIS was used in order to obtain information about the LBL modified QCM electrodes and the influence of each bilayer on the electrical properties after each layer deposition. Spectra were recorded in 0.05 M acetate +0.1 M KBr pH 5.0 buffer solution at the OCP. The EIS experiments were carried out after cyclic voltammetric experiments; therefore, we assume that electrochemical properties of the modified electrode analyzed by EIS are due to the same electroactive species, heme, which is responsible for the CV behavior.[22]

Impedance spectra are shown in Figure 6, recorded at AuQCM−MPS(−)/PDDA(+), and with {HA/Mb}$_n$, n = 2, 4, and 6; Figure 6b is a magnification of the spectra for the bilayer modified electrodes in Figure 6a. All spectra present a semicircular profile with a notably higher impedance in the case of AuQCM−MPS(−)/PDDA(+).

The equivalent circuit which best fits the spectra comprises the cell resistance, R_Ω, in series with a combination of charge-transfer resistance, R_{ct}, in parallel with a constant phase element (CPE), as a nonideal capacitor representing the double-layer capacitance, described by CPE = $\{(C\ i\omega)^\alpha\}^{-1}$, where C is the capacitance and α is an exponent which can vary between 1 for a smooth uniform surface and 0.5 for a porous electrode.[27] It is appropriate here, because the electrode was modified by sequential layers and presents a rough and heterogeneous surface.[28,29] Values of the α exponent obtained for AuQCM−MPS(−)/PPDA(+) was 0.89, and an average of α = 0.84 was calculated for AuQCM−(MPS(−)/PPD(+)/{HA/Mb}$_{1-6}$. An alternative, simpler model given the semicircular characteristics of the complex plane plots is to use a pure capacitor instead of a CPE. Figure 7 shows the R_{ct} and C_{dl} values obtained by using both modeling methods, that is, with *R*CPE and with *RC*. It can be seen that the agreement is very good; the errors associated with both calculation methods are lower than 3%, indicating that both models describe well the interfacial characteristics of the system. The advantage in the latter case is that no assumptions have to be made about the existence of the CPE.

As seen in Figure 7a, the R_{ct} value obtained for AuQCM−MPS(−)/PPDA(+) electrode is 159 kΩ cm^2 (161 kΩ cm^2 for semicircle fitting). After the deposition of the first {HA/Mb} bilayer, there is a large decrease in the charge-transfer resistance R_{ct} by a factor of 10−16 kΩ cm^2. This shows that the layers of {HA/Mb} lead to an increase in charge transfer, resulting from

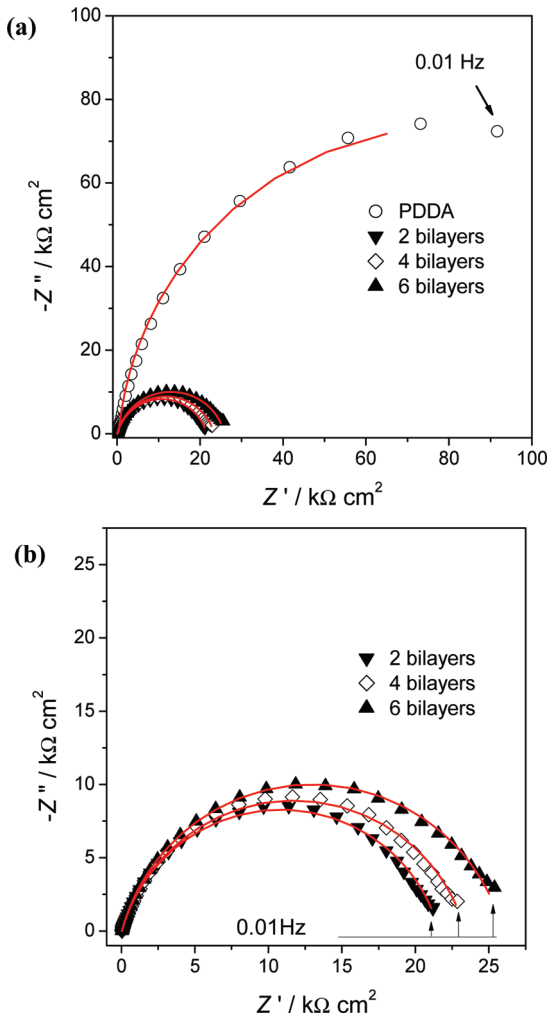

Figure 6. Complex plane impedance plots recorded at AuQCM modified electrodes in 0.05 M acetate +0.1 M KBr buffer solution pH 5.0 at the OCP; lines show equivalent circuit fitting. (a) AuQCM−MPS(−)/PDDA(+)/{HA/Mb}$_{2-6}$ and (b) amplification of the spectra for 2, 4, and 6 bilayers.

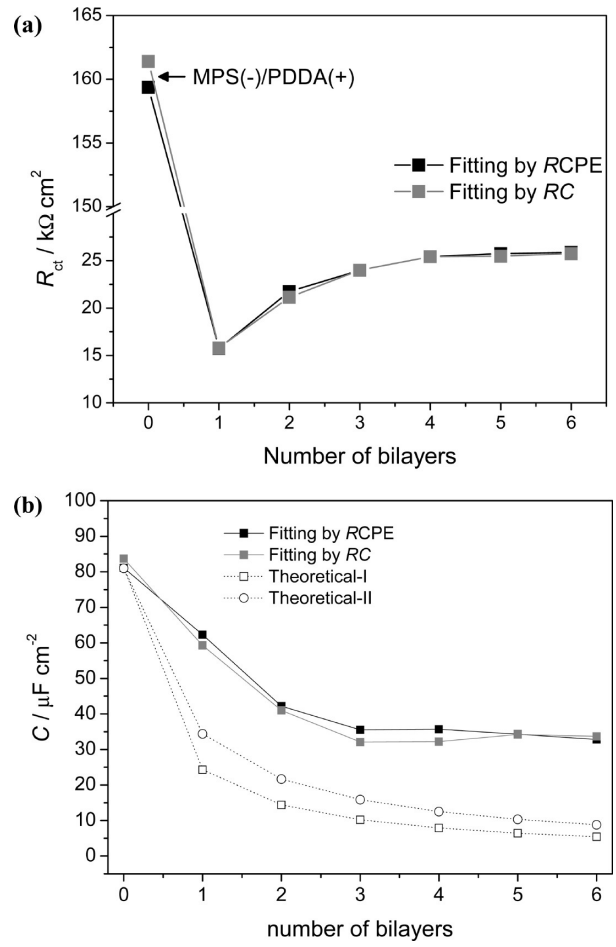

Figure 7. Parameters from impedance spectra. (a) Charge-transfer resistance values. Dark squares, from *R*CPE equivalent circuit fitting; light squares, from *RC* semicircle modeling. (b) Capacitance values. Dark squares, from *R*CPE equivalent circuit fitting; light squares, from *RC* semicircle modeling; (□) theoretical-I $C_i = 34\ \mu F\ cm^{-2}$ and (○) theoretical-II, $C_i = 59\ \mu F\ cm^{-2}$ obtained by using eq 2.

the presence of free conductive species from Mb, which have good mobility through the films, thus reaching the electrode substrate surface and increasing the electron-transfer rate. The electroactive species responsible for the electrochemical response of the modified electrode is heme, which is released during the LBL deposition because of interactions between HA and Mb. Because with each layer deposition, the diffusion of the heme through the layers is more difficult, the charge-transfer resistance increases.[22]

Further layers lead to an increase in the overall LBL film thickness, inhibiting the mobility of the electroactive species. This is reflected in an increase of the charge-transfer resistance with each bilayer, reaching 26 kΩ cm^2 with six bilayers; nevertheless, this value is substantially lower than the value at AuQCM−MPS(−)/PPDA(+).

The capacitance obtained was also the highest for AuQCM−MPS(−)/PPDA(+), $C = 81$ and 83 μF cm^2 for equivalent circuit and semicircle modeling, respectively. As expected, the capacitance value starts to decrease with the first bilayer deposition and then continues to decrease up to the third bilayer, afterward maintaining roughly the same value of $C = 34\ \mu F\ cm^{-2}$ for both modeling methods (see Figure 7b).

The total capacitance, C_t, can be understood as a series association of capacitors for each layer, as in eq 2. The higher the number of capacitors in series, the lower the total capacitance:[30]

$$c_t = \frac{1}{\frac{1}{c_1} + \frac{1}{c_2} + \ldots + \frac{1}{c_n}} \qquad (2)$$

where C_t is the total capacitance corresponding to the modified electrode with n bilayers and C_1-C_n represent the capacitance values for each individual bilayer.

We cannot easily estimate the capacitance value of each single bilayer of {HA/Mb}, owing to the fact that the films are constructed on a (surface-charged) support of AuQCM−MPS(−)/PDDA(+), and hence, it is expected that the MPS(−)/PDDA(+) layers influence the capacitance values of the first {HA/Mb} bilayers.

For modeling purposes, we first assume that the dielectric constants and thickness of each bilayer are the same, that is, a single capacitance value. A constant value of total capacitance was chosen to be $C = 34\ \mu F\ cm^{-2}$, which is that obtained after the formation of three bilayers of {HA/Mb} (see Figure 7b). By using eq 2, the capacitance value for each AuQCM−MPS(−)/PDDA(+)/{HA/Mb}$_{n=1-6}$ was calculated, shown in the Theoretical-I curve in Figure 7b. The same calculation was made with a value of capacitance $C = 59\ \mu F\ cm^{-2}$, which corresponds

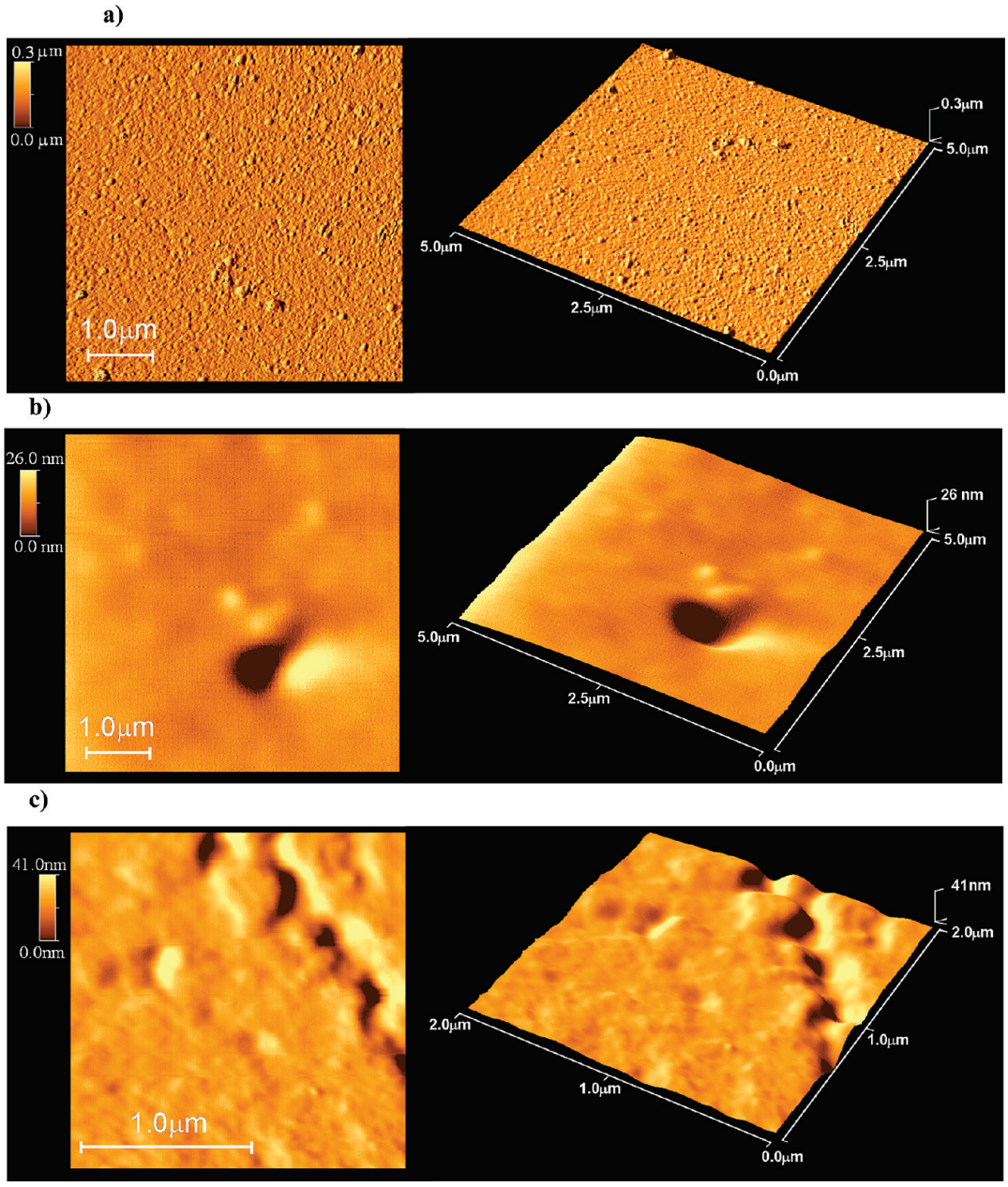

Figure 8. AFM topographical images in 2D and 3D for AuQCM−(MPS(−)/PPD(+)/{HA/Mb}$_n$, with n = (a) 2, (b) 4, and (c) 6 bilayers.

to that calculated from the AuQCM−MPS(−)/PDDA(+)/{HA/Mb}$_1$ modified electrode, that is, with one {HA/Mb} bilayer. This leads to the curve shown as Theoretical-II in Figure 7b, which is very similar to the Theoretical-I curve. It can be concluded that the value of capacitance chosen does not have a significant effect on the profile obtained.

In this type of model, the total capacitance decreases after each bilayer deposition, as expected from eq 2. Experimentally, this only occurs up to the formation of the third bilayer of (HA/Mb), when the measured capacitance reaches a constant value. This discrepancy can be ascribed to the fact that the summation in eq 2 strictly holds only for a series of pure capacitive elements, without the inclusion of a resistor connected in parallel with the CPE element.

If it is assumed that the dielectric constant of the layers is constant, the only parameter which could be responsible for the differences between the theoretical and experimental values is the thickness of the layers. The change of the electrode surface structure with each layer deposition also has to be considered. As mentioned in ref 22 and below in Section 3.4, the electrode presents island-like structures for the 1−3 bilayer LBL-modified electrodes. These islands extend with each layer deposition and then coalesce after the third bilayer. This also may explain the substantial decrease in the capacitance values, considering that the PDDA-modified electrode exhibits the highest value, which then decreases with the formation and growth of the Mb-containing islands at the electrode/solution interface. The capacitance maintains an almost constant value after deposition on the electrode surface of a uniform layer of HA/Mb. The α coefficient values, 0.81 for LBL 2, 0.83 for LBL 4, and 0.87 for LBL 6, show clearly the change in the modeled surface roughness with the deposition of layers. The homogenization of the electrode surface decreases the roughness, similar to what was obtained in other studies with LBL {HA/CHI} and {HA/PDDA} films.[17,31]

The impedance results are in agreement with what was observed in the QCM gravimetric experiments, supporting the decrease in friction at the solution/electrode interface and

reinforcing the supposition that surface roughness decreases after LBL formation, confirmed also by the AFM imaging presented below.

3.4. AFM. Contact-mode AFM was used to examine the local morphological structures of modified AuQCM/(MPS(−)/PPD(+)/{HA/Mb}$_n$ electrodes. Figure 8 shows 2D and 3D images of the AuQCM−MPS(−)/PDDA(+)/{HA/MB}$_n$ modified electrodes, with $n = 2$, 4, and 6. The difference in the resolution of AFM images is due to the fact that, for films with a greater number of bilayers, the curvature of the surface and the electrostatic charge accumulated on the surface hindered the operation, interfering with cantilever movement and therefore with the measurement. In order to obtain parameters to compare the surface changes after formation of each bilayer, the mean roughness was calculated.

AFM showed that the morphology of the modified electrode surface differs from one layer to another. Figure 8a shows the rougher surface of the AuQCM electrode after formation of 2 bilayers: as can be seen, the crystal surface is covered with small nanostructures, homogeneously distributed across the surface. Figure 8b,c demonstrates that, with the deposition of further layers, $n = 4$ and 6, the empty spaces and the pores become filled, the surface starts to become smoother, and the nanostructure begins to fade. Nevertheless, a small amount of porosity can still exist, as purposely shown in Figure 8b for $n = 4$; no evidence of this continuing up to $n = 6$ was seen (Figure 8c).

The decrease in surface roughness is in agreement with analysis of the data obtained by EQCM and EIS, explaining the observed reduction in friction in the electrode−liquid interface. We suppose that the formation of the first layer is nonuniform and presents structures such as islands throughout the surface, randomly distributed. With each layer deposition, the surface becomes smoother; but the process does not follow a predefined profile, in agreement with what was also reported in the literature.[17,32] The films formed may still have some holes, as can be seen in Figure 8b, which shows the AuQCM covered by four bilayers, because it is possible to see the valleys and cracks. This observation is the same for six bilayers, see Figure 8c.

In principle, the process of washing and drying could influence the film morphology, including the formation of structures, such as scars, islands, and failures. The cleaning process, using water and then N_2, could lead to failures in smoothness of the surface. However, according to the literature, HA forms a vitreous film with well known elasticity and resistance to cracking,[34] which leads us to believe that the formation of such structures is unlikely.

The mean roughness, R_a, is defined as the absolute average deviation of the roughness irregularities from the mean line over one sampling length.[33] The calculated roughness parameter obtained for two bilayers was $R_a = 2.87$ nm, decreasing to $R_a = 1.32$ nm for four bilayers and $R_a = 1.12$ nm for six bilayers. This is reflected also in the increasing CPE exponents in impedance spectra discussed in the previous section (0.81, 0.83, and 0.87, respectively).

The information obtained from the AFM images is in agreement with what was obtained in the QCM and EIS studies. It is seen that the formation of the initial layers occurs randomly and heterogeneously over the surface, and then, the surface becomes smoother and more homogeneous after each layer formation. The complementary combination of the various techniques is valuable for the elucidation of such mechanisms.

4. Conclusions

The LBL film formation process of HA with Mb has been monitored by QCM, giving important information about the mechanism of film assembly, successfully carried out onto an Au electrode surface. The gravimetric data show that the mass deposited does not grow linearly, neither does it grow exponentially, with each layer deposition, as seen in some reports in the literature. Both gravimetric and voltammetric results show that the {HA/Mb}$_n$ films have very good stability in terms of structure and electroactivity over a long period of time.

Impedance spectra confirm the electroactivity of the films, the first {HA/Mb} bilayer exhibiting a lower charge-transfer resistance than the precursor MPS(−)/PDDA(+) modified electrode. The formation of sequential {HA/Mb}$_n$ up to six bilayers results in an increase of the total charge-transfer resistance of the {HA/Mb}$_n$ modified electrodes, in agreement with cyclic voltammetry, with the total capacitance reaching an almost constant value after three bilayers because of differences between, and possible reorganization of, the layers within the multilayer film structure. AFM imaging shows that the {HA/Mb} films formed on the electrode surface become smoother with each layer deposition, in agreement with what was observed in the QCM and EIS studies.

It has been shown that the combination of EQCM monitoring of the LBL film deposition, EIS and AFM, can give valuable information about the multilayer deposition mechanism and about how the interaction of species contained within each layer can influence the overall characteristics of the {HA/Mb}$_n$ film. The approach described here can be applied for examining the construction of other self-assembled monolayer or bilayer films and help elucidate the properties of this type of electroactive thin layer structure.

Acknowledgment. Financial support from Fundação para a Ciência e a Tecnologia (FCT), PTDC/QUI/65255/2006 and PTDC/QUI/65732/2006, POCI 2010 (cofinanced by the European Community Fund FEDER) and CEMUC® (Research Unit 285), Portugal, is gratefully acknowledged. FCT is thanked for PhD grants for E.M.P. (SFRH/BD/31483/2006) and M.M.B. (SFRH/BD/27864/2006). The authors thank Wyllerson Gomes, Luiz Bonugli, and Profs David Soares and Omar Teschke, IFGW Unicamp Brazil, for technical help and scientific discussions.

References and Notes

(1) Decher, G.; Hong, J. D.; Schmitt, J. *Thin Solid Films* **1992**, *210*, 831–835.
(2) Decher, G. *Science* **1997**, *277*, 1232–1237.
(3) Decher, G.; Hong, J. D. *Makromol. Chem., Macromol. Symp.* **1991**, *46*, 321–327.
(4) Lvov, Y. In *Protein Architecture: Interfacing Molecular Assemblies and Immobilization Biotechnology*; Lvov, Y., Mohwald, H., Eds.; Marcel Dekker: New York, USA, 2000; pp 125−167.
(5) Lvov, Y.; Munge, B.; Giraldo, O.; Ichinose, I.; Suib, S.; Rusling, J. F. *Langmuir* **2000**, *16*, 8850–8857.
(6) Ma, H.; Hu, N.; Rusling, J. F. *Langmuir* **2000**, *16*, 4969–4975.
(7) Chapin, M. F.; Bucke, C. *Enzyme Technology*; Cambridge University Press: Cambridge, UK, 1990.
(8) Laurent, T. C.; Fraser, J. R. E. *FASEB J.* **1992**, *6*, 861–870.
(9) Burke, S. E.; Barett, C. J. *Biomacromolecules* **2005**, *6*, 1419–1428.
(10) Kim, T. G.; Lee, H.; Jang, Y.; Park, T. G. *Biomacromolecules* **2009**, *10*, 1532–1539.
(11) Lu, H.; Hu, N. *J. Phys. Chem. B* **2006**, *110*, 23710–23718.
(12) Page, C. C.; Moser, C. C.; Chen, X.; Dutton, P. L. *Nature* **1999**, *402*, 47–51.
(13) Johansson, J. A.; Halthur, T.; Herranen, M.; Soderberg, L.; Elofsson, U.; Hilborn, J. *Biomacromolecules* **2005**, *6*, 1353–1359.
(14) Schoeler, B.; Poptoshev, E.; Caruso, F. *Macromolecules* **2003**, *36*, 5258–5264.

(15) DeLongchamp, D. M.; Kastantin, M.; Hammond, P. T. *Chem. Mater.* **2003**, *15*, 1575–1586.
(16) McAloney, R. A.; Sinyorr, M.; Dudnik, V.; Goh, M. C. *Langmuir* **2001**, *17*, 6655–6663.
(17) Picart, C.; Lavalle, P.; Hubert, P.; Cuisinier, F. J. G.; Decher, G.; Schaaf, P.; Voegel, J.-C. *Langmuir* **2001**, *17*, 7414–7424.
(18) Lavalle, P.; Picart, C.; Mutterer, J.; Gergely, C.; Reiss, H.; Voegel, J.-C.; Senger, B.; Schaaf, P. *J. Phys. Chem. B* **2004**, *108*, 635–648.
(19) Elbert, D. L.; Herbert, C. B.; Hubbell, J. A. *Langmuir* **1999**, *15*, 5355–5362.
(20) Picart, C.; Mutterer, J.; Richert, L.; Luo, Y.; Prestwich, G. D.; Schaaf, P.; Voegel, J.-C.; Lavalle, P. *Proc. Natl. Acad. Sci. U.S.A.* **2002**, *99*, 12531–12535.
(21) Richert, L.; Lavalle, P.; Payan, E.; Zheng, X. S.; Prestwich, G. D.; Stoltz, J. F.; Schaaf, P.; Voegel, J.-C.; Picart, C. *Langmuir* **2004**, *20*, 448–458.
(22) Barsan, M. M.; Pinto, E. M.; Brett, C. M. A. *Electrochim. Acta* **2010**, *55*, 6358–6366.
(23) Hoogvliet, J. C.; van Bennekom, W. P. *Electrochim. Acta* **2001**, *47*, 599–611.
(24) Sauerbrey, G. *Z. Phys.* **1959**, *155*, 206–222.
(25) Arnau, A., Ed. *Piezoelectric Transducers and Applications*; Springer-Verlag: Berlin, 2004.
(26) Rodahl, M.; Hook, F.; Fredriksson, C.; Keller, C. A.; Krozer, A.; Brzezinski, P.; Voinova, M.; Kasemo, B. *Faraday Discuss.* **1997**, *107*, 229–246.
(27) Brett, C. M. A.; Oliveira Brett, A. M. *Electrochemistry. Principles, methods and applications*; Oxford University Press: Oxford, 1993.
(28) Barsan, M. M.; Pinto, E. M.; Florescu, M.; Brett, C. M. A. *Anal. Chim. Acta* **2009**, *635*, 71–78.
(29) Pinto, E. M.; Gouveia-Caridade, C.; Soares, D. M.; Brett, C. M. A. *Appl. Surf. Sci.* **2009**, *255*, 8084–8090.
(30) Barsoukov, E.; Macdonald, J. R., Eds. *Impedance Spectroscopy; Theory, Experiment, and Applications*, 2nd ed.; Wiley Interscience Publications: New York, 2005.
(31) Cui, X.; Li, C. M.; Bao, H.; Zhen, X.; Lu, Z. *J. Colloid Interface Sci.* **2008**, *327*, 459–465.
(32) Liu, H.; Hu, N. *J. Phys. Chem. B* **2006**, *110*, 14494–14502.
(33) Gadelmawla, E. S.; Koura, M. M.; Maksoud, T. M. A.; Elewa, I. M.; Soliman, H. H. *J. Mater. Process. Technol.* **2002**, *123*, 133–145.
(34) Lapčik, L., Jr.; Lapčik, L. *Chem. Rev* **1998**, *98*, 2663–2684.

JP107107B